J Porous Mater (2018) 25:63–73
DOI 10.1007/s10934-017-0421-2

Facile tailoring of hierarchical mesoporous AlSBA-15 by ionic liquid and their applications in heterogeneous catalysis

Hassan M. A. Hassan[1] · Mohamed A. Betiha[2] · Reda F. M. Elshaarawy[1] · Emad A. Ahmed[1]

Published online: 9 April 2017

Abstract Significant enhancement in the performance of incorporation of high content of aluminum within hierarchical mesoporous SBA-15 has been achieved by direct route using urea tetrachloroaluminate ionic liquid as novel aluminum source. The fabricated materials were fully characterized by N_2 sorption isotherms, powder X-ray diffraction (XRD), FT-IR, ^{27}Al MAS NMR, XRF, HRTEM and FESEM. The acidic properties of these materials have been examined using NH_3-TPD. The catalytic performance was investigated using cumene cracking and the esterification reaction as a probe molecules to estimate the acidity of the material. It is worth noting that the ionic liquid with accomplished Al–O–Si bonds is an efficient precursor to synthesis AlSBA-15 with high aluminum content (nSi/mAl = 7) without destroying the structural order of the material in acidic medium. ^{27}Al MAS NMR spectra of AlSBA-15 show that all aluminum species were incorporated into the SBA-15 framework with nSi/mAl ratio up to 7. Overall, this work emphasize that the AlSBA-15 materials contain Bronsted and Lewis acid sites with medium acidity which makes them adequate to be adopted as acid catalysts in heterogeneous catalysis.

Keywords AlSBA-15 · Various Si/Al ratio · Ionic liquid · Cumene cracking · Esterification reaction

✉ Hassan M. A. Hassan
hassan.hassan@suezuniv.edu.eg

✉ Mohamed A. Betiha
mohamed_betiha@hotmail.com

[1] Department of Chemistry, Faculty of Science, Suez Canal University, Suez, Egypt

[2] Egyptian Petroleum Research Institute, Nasr City, Cairo 11727, Egypt

1 Introduction

The development of mesoporous materials with high specific surface areas, relatively uniform pore size and high chemical stability is currently an area of tremendously expanded research, particularly with regard to potential applications in areas such as adsorption, metal ions separation, and sensor technology [1–5]. Besides these applications, these mesoporous materials considered a promising candidate in catalysis [6–14]. Acid-catalyzed reactions are very widespread and essentially in industrial applications such as petrochemical industry, oil refining and pharmaceutical synthesis. Zeolites are immensely used as solid acid catalysts, especially in the petrochemical industry and oil refining [15]. However, their microporous nature restricts the applications and make them inappropriate for a large organic molecules processing [16]. Therefore, seeking proper materials to meet this challenge is of great interest. Recently, Mesoporous silica as those of M41S, SBA-n and MSU-X families is being developed and attracted attention as a promising class of materials to be used as catalytic support. This family of materials is characterized by order array of pores with well-uniform diameter, high specific surface areas, and pore volumes, which are beneficial for the acid catalyzed reactions using bulky molecules. However, mesoporous silica do not display the same acidity and lack of acid sites when compared with crystalline zeolite. This can be attributed to the amorphous character of their pore walls. In spite of this, many research groups have supposed that Al-incorporated ordered mesoporous silica offers strong Brønsted acidity and are useful large-pore alternatives for zeolites acid catalysis [17–21]. Therefore, the ability to design materials with monitoring the chemical composition and definite pore structure represents a timely topic in catalysis research. The incorporation of Aluminum

within the amorphous silica walls is imperative for the production of mesoporous materials with well-distributed active site. Obviously, the strength of the acid sites could be varied with changing the nature and number of trivalent framework cations. Materials with regular and definite pore sizes are anticipated to play significant role in the acid-catalyzed reactions. Among mesoporous structure support with regular pores, SBA-15 appear to be more proper to exploit in organic transformation reactions because SBA-15 has larger pore sizes (4.6–30 nm), thicker pore walls (3.1–6.4 nm) and higher surface area (up to 1000 m^2/g). For SBA-15 to be exploited as a catalyst in acid catalyzed reactions, acid sites require to be grafted, to offer a remarkable enhancement in the acid strength of SBA-15. Thus, the grafting of metal ions, such as aluminum, in the silica matrix is necessary for the production of catalytically acid sites. The main problem for the synthesis of AlSBA-15 is the highly acidic synthesis condition is required for the formation of SBA-15 where aluminum is sitting as soluble species that are not graft in the silica framework. Therefore, finding a facile and ecofriendly method to synthesize aluminum-containing SBA-15 is of interest.

In the present work, we report the fabrication of AlSBA-15 under mild acidic conditions using urea-tetrachloroaluminate as a novel aluminum source. The synthesis was performed through adjusting the molar $nH_2O/nHCl$ ratio, which indicates the formation of Si–O–Al linkages that lead to isomorphous substitution of Si^{4+} by some Al^{3+}. A series of different AlSBA-15 materials with various nSi/mAl ratio have been synthesized.

2 Experimental

2.1 Synthesis of protonated urea tetrachloroaluminate

A certain amount of urea and equivalent amount of 1 M HCl were stirred at room temperature for 1 h under nitrogen gas [22]. A required molar weight of anhydrous aluminum chloride was added to urea hydrochloride mixture and was thoroughly stirred for 1 h.

2.2 Direct-synthesis aluminated AlSBA-15(n)

In typical synthesis, 4 g of Pluronic P123 was added to 30 g of water with stirring for 4 h to obtain a clear solution. Subsequently, 70 mL of 0.29 M HCl was added and the solution was stirred for another 2 h (pH, ca. 2.2). Then 9.0 g of TEOS and an appropriate amount of urea tetrachloroaluminate were added directly into the homogeneous solution under stirring with changing the amount urea tetrachloroaluminate to give different nSi/mAl ratio denoted AlSBA-15(n), where n is 3, 7, and 15 (Scheme 1). The as synthesized aluminated SBA-15 were aged at 100 °C for 24 h. The obtained solid was filtrated, washed with water thoroughly and dried in air at 120 °C for 12 h. The product was finally calcined at 550 °C for 6 h to obtain AlSBA-15(3), AlSBA-15(7), and AlSBA-15(15).

2.3 Characterization methods

FT-IR spectra of the samples were carried out using ATI Unicam (Mattson 936) spectrometer. X-ray diffractograms were obtained on a XPERT X-ray diffractometer, operating with CuKα radiation (λ = 0.1542 nm), X-ray radiation (X-ray generator current and voltage set at 40 mA and 45 kV). The diffractograms were recorded in the 2θ range of 0.5 to 10° with a 2θ step size of 0.01° and a step time of 10 s. X-ray fluorescence (XRF) was used to quantify Si/Al ratios of the samples operated at 20 mA and 50 kV using a Bruker (S4 EXPLORER). Nitrogen adsorption and desorption isotherms were measured at (−196 °C) using a NOVA 3200 system (USA). Prior to the analysis, the samples were outgassed at 300 °C for 3 h. The specific surface areas were calculated by using the Brunauer–Emmett–Teller (BET) model. The pore size distributions were obtained using the adsorption branch of the nitrogen isotherms by applying the Barrett–Joyner–Halenda (BJH) method. Transmission electron microscopy (HRTEM) images were obtained using a JEOL 2011 electron microscope (Japan) operated at 200 kV. The morphology of the samples was investigated using a field emission scanning electron microscope (FESEM). Temperature programmed desorption (NH_3-TPD) of ammonia was measured using a CHEMBET 3000 chemical absorber (Quantachrom). Samples were activated at 500 °C for 1 h in a flow of helium; subsequently ammonia was introduced for 1.5 h at 100 °C. The physically adsorbed ammonia molecules were removed by purging with helium flow until the baseline was flat, then the reactor temperature was increased to 700 °C with a ramping rate of 10 °C /min. Solid-state ^{27}Al MAS NMR spectra were recorded at room temperature on a Bruker DRX-400 spectrometer equipped with a magic angle spin probe.

2.4 Catalytic activity

2.4.1 Cumene cracking

Cumene cracking experiments were carried out in a micro-activity-reference unit (PID Eng & Tech, Spain). A fixed-bed tubular reactor (autoclave engineers) was made of a 505 mm length, 19 mm outer diameter, 13.1 mm inner diameter tube (Inconel 600) that was heated with a reactor furnace and integrated within the hot box. The liquid reactant was introduced into the unit using a HPLC positive alternative displacement pump (Gilson, model 307). The

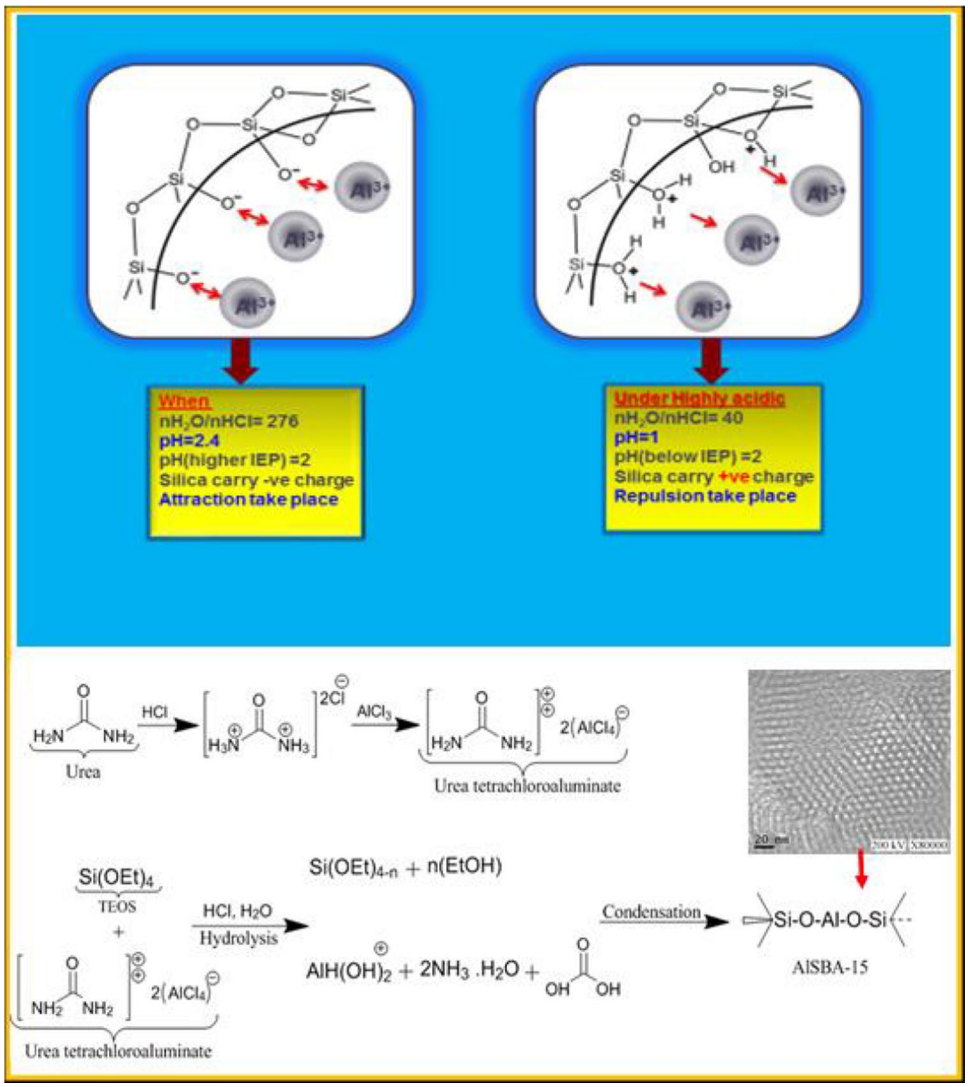

Scheme 1 The synthesis of periodically ordered mesoporous AlSBA-15 using urea tetrachlorometalate

gas source in this experiments was N_2, which was fed to the system through an electronic HI-TEC mass-flow controller (Bronkhorst, model EL-FLOW). Before reaction, the catalysts were in situ dried under N_2 (20 mL/min) for 2 h at 400 °C. After the materials activation, the reaction temperature was adjusted at the required operating temperature and catalytic test was carried out at atmospheric pressure. Experimental conditions of cumene cracking are; liquid hourly space velocity (LHSV; W/W), was fixed at 2.5 h^{-1}, N_2/cumene ratio = 20 mL/mL, atmospheric pressure.

2.4.2 Esterification reaction

The esterification of acetic acid reaction was carried out by taking 1 wt% of the activated sample (pre-heated at 300 °C for 3 h) with required amount of acetic acid and butanol (1:1) at 80 and 100 °C in a 100 mL round-bottomed flask equipped with a reflux condenser. Aliquots of the reaction mixture were collected at different time intervals and analyzed by GC (Agilent Technologies, model 6890 N, capillary column HP-5, 30 m, containing 5% methyl + 95% phenyl siloxane). Conversion was defined as the percentage of acetic acid consumed and estimated from gas chromatographic analysis.

3 Results and discussion

3.1 Characterization of the materials

The mesoporous SBA-15 materials were synthesized under strongly acidic hydrothermal conditions ($nH_2O/nHCl = 40$, i.e., pH 1). Under these conditions, the direct incorporation of a large amount of Al^{3+} ions into the SBA-15 materials is very harsh. This could be mainly due to the solubility of the Al precursor is very high in acidic medium and exists only in the cationic form rather than its corresponding oxo species. Therefore, Al atoms cannot be grafted

into the protonated mesoporous walls via a condensation process with silicon species owing to the quite high repulsion between the positively charged Al oxo species and the cationic silica species at lower pH. However. In our previous work, endeavor were made to adjust the ideal ratio of nH_2O/nHCl. It was found that when the nH_2O/nHCl ratio of 276 was used the pH of the synthesis mixture was about 2.4, which is higher than the isoelectric point of silica, consequently the silica species acquire negative charge, which supports the interaction with the negatively charged silica species and positively charged Al oxo species $Al(OH)_2^+$ (Scheme 1). Therefore, nH_2O/nHCl ratio of 276 was found to be the suitable ratio for AlSBA-15 preparation and improved the amount of Aluminum grafting into the SBA-15 walls. The elemental analysis of the synthesized AlSBA-15 via urea-tetrachloroaluminate as the Al precursor with different molar ratio of nSi/mAl in the initial gel at nH_2O/nHCl ratio of 276 are listed in Table 1. A set of experiments with various molar ratio of nSi/mAl in the initial gel mixture are applied for the synthesis of AlSBA-15 using urea-tetrachloroaluminate as aluminum source. The results revealed that there is a variation in the nSi/mAl ratio of the product materials as a function of nSi/mAl in the initial gel. These results emphasized that the urea-tetrachloroaluminate precursor with preformed Al–O–Si bonds is an efficient precursor to prepare AlSBA-15 with high aluminum content under acidic conditions.

FT-IR spectra of AlSBA-15 materials with various nSi/mAl ratio are depicted in Fig. 1. In all cases, the predominance peak at about 1093 cm^{-1} are assigned to the asymmetric stretching of Si–O–Si groups. The symmetric stretching of the same groups take place at about 815 and 600 cm^{-1} while, the peak at around 455 cm^{-1} correspond to the Si–O–Si or Al–O–Si bending vibration mode. The band at about 965 cm^{-1} is assigned to the presence of defective Si–OH groups [23]. The presence of these bands in our samples manifests the grafting of aluminum into SBA-15 frameworks. In addition, all samples depict a broad

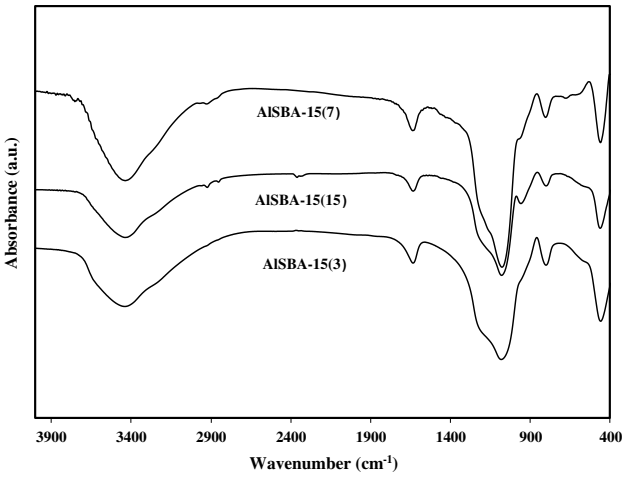

Fig. 1 FTIR spectra of AlSBA-15 materials synthesized at different nSi/mAl ratios

absorption band at 3700–3300 cm^{-1} corresponding to the exciting of hydrogen bond (H–O–H) and SiO–H groups. Aluminum incorporation into SBA-15 with nSi/nAl of 7 leads to the presence of a weak band at 3625 cm^{-1}. This band is assigned to the OH stretching vibration of zeolite-type Si–OH–Al groups of the mesoporous aluminosilicate [24]. The band around 3770 cm^{-1} is significant decreased with increasing aluminum content due to decrease isolated Si–O–Al species. The AlSBA-15 with nSi/nAl of 3, results in a remarkable decrease of isolated silanol species as observed by the reduced intensity of the 3770 cm^{-1} band. It worth noting that high content of aluminium results in an amendment of the most tetrahedron surface silanol groups of the SBA-15 original sample [25].

The powder XRD patterns of AlSBA-15 samples prepared using urea-tetrachloroaluminate as the Al precursor with different molar ratio of nSi/mAl are presented in Fig. 2a. The materials AlSBA-15(7), and AlSBA-15(15), depict well-resolved XRD patterns assigned to typical

Table 1 Texture properties of AlSBA-15 materials synthesized at various *n*Si/*n*Al ratios

Sample	*n*Si/*n*Al in gel	*n*Si/*n*Al in product[a]	a_0/nm[b]	$A_{BET}/(m^2g^{-1})$[c]	$V_P/(cm^3/g)$[d]	D_P/ads/nm[e]	*W*/(nm)[f]
SBA-15	–		11.62	876	1.06	7.4	4.22
AlSBA-15(3)	3	5	15.0	319	0.61	9.7	5.3
AlSBA-15(7)	7	9	13.05	813	1.20	8.2	4.68
AlSBA-15(15)	15	20	12.58	805	1.23	8.96	3.62

[a]Si/Al ratios in final products were obtained by XRF

[b]Unit cell parameter calculated by ($a_o = 2d_{100}/\sqrt{3}$)

[c]Surface area (BET)

[d]Total pore volume

[e]Mean pore diameter (BJH)

[f]Wall thickness, calculated by (a_o—pore diameter)

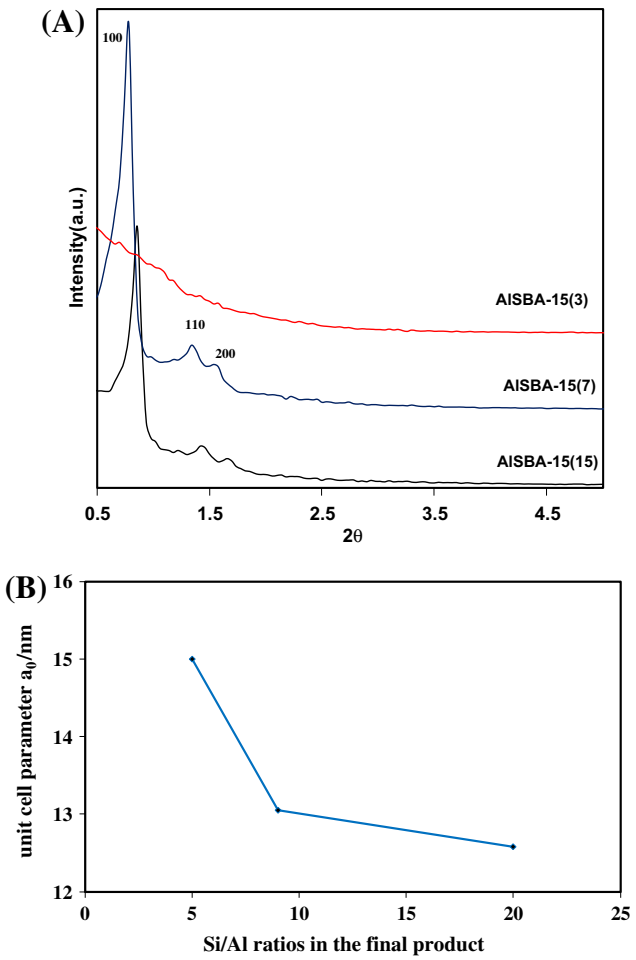

Fig. 2 **a** XRD powder patterns of AlSBA-15 materials synthesized at various *n*Si/*m*Al ratios. **b** The unite cell parameter of AlSBA-15 as a function of aluminum content

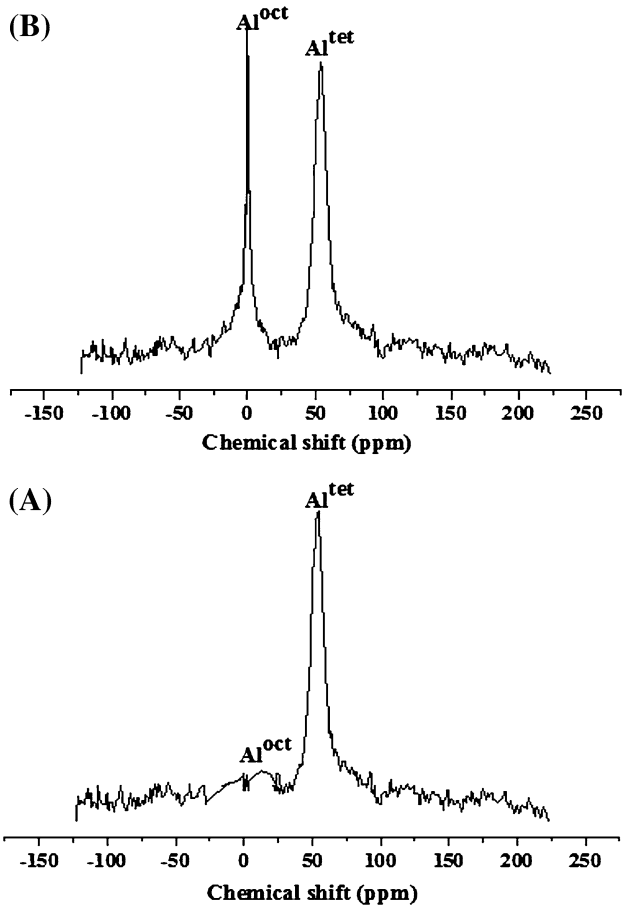

Fig. 3 ^{27}Al MAS NMR spectra of AlSBA-15 synthesized at different nSi/mAl ratios (*a*) AlSBA-15(7) and (*b*) AlSBA-15(3)

SBA-15 structures, confirming that high-quality SBA-15 materials are obtained and the hexagonal structure was not affected by these treatments [26, 27]. It was found that they exhibit three well-defined peaks, which are indexed as (1 0 0), (1 1 0), and (2 0 0) reflections indicating that these samples are characterized by P6mm hexagonal symmetry, typical of pure SBA-15 mesostructure. However, no obvious ordered arrangement of the mesopores could be found and the structure order of the samples deteriorates with increasing the aluminum contents up to nSi/mAl ratio of three. Interestingly, the intensity of the reflections increases with decreasing nSi/mAl ratio, except for AlSBA-15(3). This indicates that the order arrangement was enhanced with Al grafting within the SBA-15 framework. In case of the sample AlSBA-15(7), the (1 1 0) reflection is very well declared whereas the intensity of the higher reflections is reduced [28, 29]. The unit cell parameters of the AlSBA-15 materials increase with the decreasing of nSi/mAl ratios. This result indicates that the materials syhthesized with the single molecular precursor tend to have large unit cell parameter (Fig. 2b). Additionally, the lattice of AlSBA-15 samples is expanded, this could be attributed to the ionic radii of Al^{3+} (0.039 nm) are bigger than that of Si^{4+} (0.026 nm). Isomorphous substitution of Si^{4+} by Al^{3+} ions mostly results in an increase in unit cell parameter that is consistent with the presence of Al^{3+} ions in the framework or in the silica pore walls. Obviously, all these described observation suggest that well-dispersed Al^{3+} ions in the lattice with no isolated Al_2O_3 clusters was formed.

The ^{27}Al MAS NMR spectra of calcined AlSBA-15 samples with different nSi/nAl ratios are displayed in Fig. 3. It worth noting that the coordination of Al significantly influenced with changing nSi/mAl ratio in the fabricated materials. Obviously, the sample synthesized with nSi/ mAl ratio of 7 (AlSBA-15(7)) displays a single sharp peak at 52 ppm assigned to framework aluminum confirming that almost all aluminum species are in tetrahedral coordination sphere. However, the spectrum of the sample with nSi/mAl ratio amounts to 3 [AlSBA-15(3)] shows two peaks at 0 and 52 ppm. The peak at 52 ppm is attributed to framework

aluminum species in tetrahedral coordination sphere while, the peak at 0 ppm are assigned to octahedral aluminum corresponding to extra-framework aluminum species. Further emphasize of the incorporation of Aluminum into SBA-15 framework is also obtained from the elemental analysis. It was found that the amount of aluminum in AlSBA-15(7) is less than that AlSBA-15(3) (Table 1).

Information on the porosity and the textural characteristics of AlSBA-15 were acquired from nitrogen adsorption isotherms at (77 K) which permit the calculation of specific surface area, pore volume and pore radius. Figure 4 displays the adsorption–desorption isotherms and pore size distribution of AlSBA-15 with different nSi/mAl ratios and a synopsis of the textural characteristics of the samples are presented in Table 1. As indicated, the adsorption isotherms of the samples AlSBA-15(7), and AlSBA-15(15) are of type IV according to IUPAC classification and displayed a H1 broad hysteresis loop at high relative pressure, indicating that AlSBA-15 has orderly mesoporous regardless of their large pore size, which was also confirmed by its cramped pore size distribution (see insert) [30]. All isotherms exhibit a sharp steepness characteristic of capillary condensation of nitrogen within regular mesopores at the relative pressure approximately ($p/p_o > 0.65$), where the p/p_o position of the inflection point is correlated to the diameter of the mesopore. As SBA-15 and AlSBA-15 has a hexagonal arrangement of mesopores connected by smaller micropores [31, 32], it is obvious that the broad hysteresis loop in the isotherms of the samples reflects the long mesoporous, which control the emptying and filling the accessible volume. However, the opposite effect has been observed when AlSBA-15 is prepared with nSi/mAl ratio of three. It is explicit that the isotherm displays type IV isotherm pattern with less declared capillary condensation step, implying less ordered mesostructure, which is in good agreement

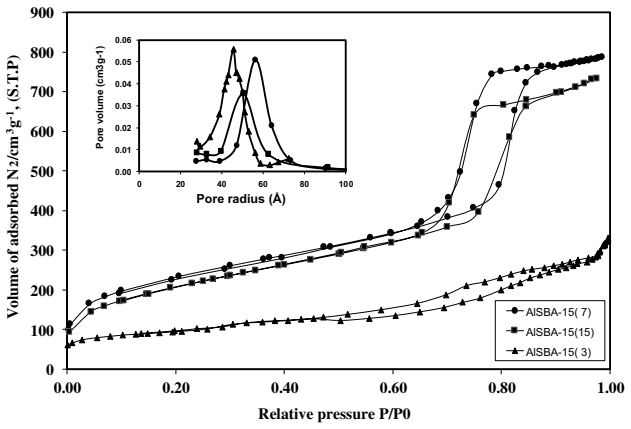

Fig. 4 Nitrogen adsorption isotherms AlSBA-15 materials synthesized at different nSi/mAl ratios. The *inset* shows the pore size distribution

with the XRD results. Moreover, the specific surface area of the sample with Si/Al = 3 is about 319 m^2/g with large pore diameter (~9.7 nm calculated from the adsorption branch of the isotherm) and pore volume (~0.6 cm^3/g). The AlSBA-15(3) sample displayed pore diameter higher than AlSBA-15(7), and AlSBA-15(15). However, the same sample showed thicker walls (5.3 nm) with respect to the other nSi/mAl ratios. These data suggest that AlSBA-15 with the nSi/nAl ratio of 3 led to the formation of a more condensed structure. Moreover, all samples prepared with various nSi/mAl ratios from 7 to 3 possess higher pore volume as compared to those of the pristine SBA-15 thus indicating in a high portion of ultramicroporous in the AlSBA-15 samples [33]. This revealed that AlSBA-15 could be synthesized with very high aluminum content (nSi/mAl = 7) without destroying the structural order of the material.

Transmission electron images of the synthesized AlSBA-15 are shown Fig. 5, which additionally boost the fine periodicity of mesopores in these materials. The TEM images of AlSBA-15(7), and AlSBA-15(15), display well-ordered hexagonal array of the mesoporous channels implying that these samples have a *2D P6mm* hexagonal structure, as does SBA-15. However, no order arrangement of the mesoporous could be observed for AlSBA-15(3). These results indicate that the structural order of the materials deteriorates with increasing the aluminum contents in the materials, which is in good agreement with XRD results.

FESEM for the series of the synthesized AlSBA-15 materials with different nSi/mAl ratios are manifested in Fig. 6. It worth noting that the morphology of AlSBA-15(3), AlSBA-15(7) and AlSBA-15(15) samples fabricated using urea-tetrachloro- aluminate as the Al source show similar particle morphology. AlSBA-15(7) and AlSBA-15(15) showed polygonal shaped particles with a small and uniform size. Whereas, AlSBA-15(3) is comprised of monodispersed aggregates, whose average particle size were greater than 500 nm. The hug lowering in the particles size of AlSBA-15 upon using urea-tetrachloroaluminate as the Al^{3+} precursor with different molar ratio of nSi/mAl could be attributed to the ability of ionic liquid to dissolve the nonionic surfactants.

The acidity of AlSBA-15 with nSi/mAl ratios of 3, 7, and 15 was measured by NH_3-TPD technique. Figure 7a depicts the NH_3-TPD profiles of AlSBA-15(3), AlSBA-15(7) and AlSBA-15(15) and the total number of acid sites obtained from NH_3-TPD are collected in Table 2. The NH_3-TPD profiles of the calcined AlSBA-15 show desorption peaks of NH_3 in the range of 100 to 550 °C, assigned to the acidic sites with medium strength. The peaks has been resolved into three distinct peaks. First, a low desorption temperature peak can be attributed to physisorbed ammonia or NH_3 hydrogen bonded to terminal silanol groups [34, 35]. Secondly, a peak distributed over the range of 300 and

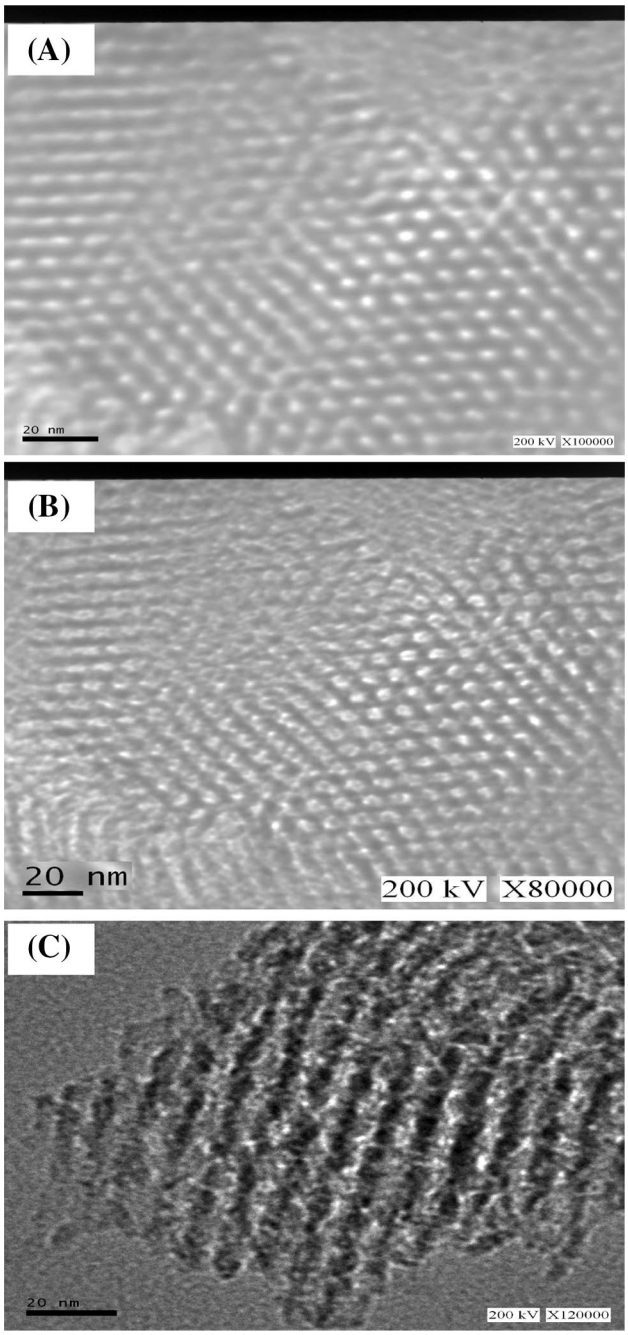

Fig. 5 HRTEM images of (**a**) AlSBA-15(15), **b** AlSBA-15(7), and **c** AlSBA-15(3) materials with different nSi/mAl ratios

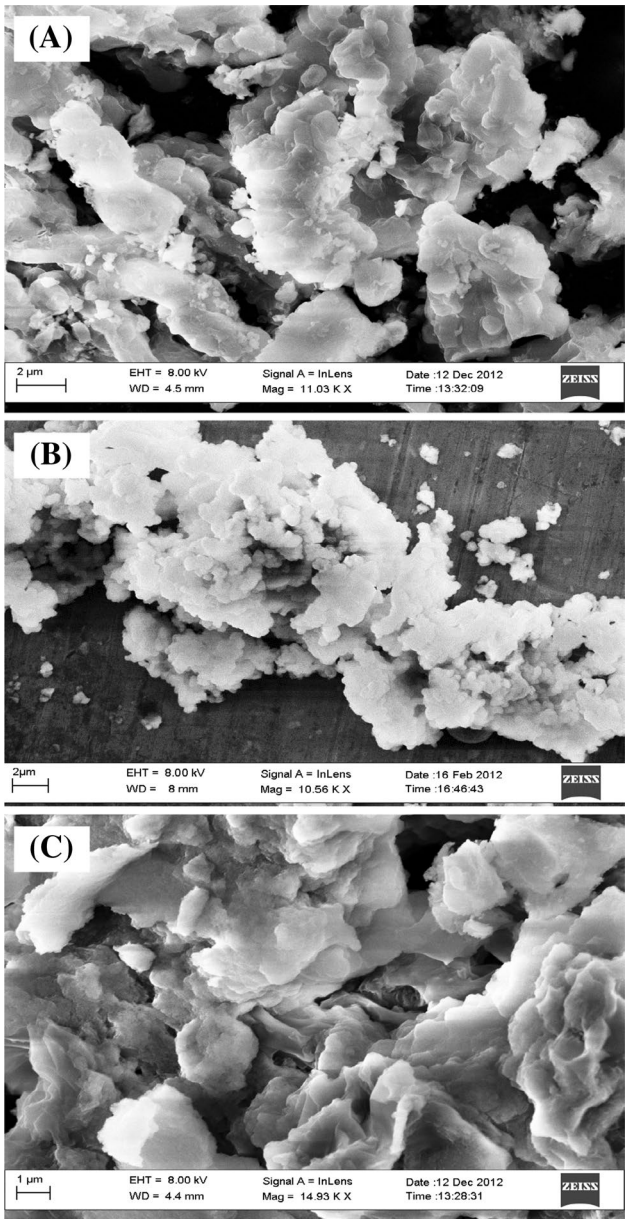

Fig. 6 FESEM images of (**a**) AlSBA-15(15), **b** AlSBA-15(7) and **c** AlSBA-15(3) materials with different nSi/mAl ratios

400 °C ascribed to ammonia adsorbed on Al in the framework of AlSBA-15 samples. Finally, the peak at higher desorption temperature was assigned to the extra-framework Al. In case of all samples, the total acidity is not as high as the difference of the aluminum content and the amount of acid sites does not run parallel with the aluminum content. Generally, the content of acidic sites of zeolite increases with the aluminum content. However, this is not the case for AlSBA-15 with nSi/mAl ratios lower than **7**. Additionally, the total number of acid sites calculated from NH_3-TPD allows the total acidity of these materials to arrange as; AlSBA-15(7) > AlSBA-15(15) > AlSBA-15(3). The thick and amorphous pore wall of the mesoporous materials could explain the observed results. Some of the aluminum atoms in AlSBA-15 are grafted in the thick wall, which are not accessible to the probe molecule. From the above analysis, we can know that the acidic properties of the mesoporous aluminosilicates cannot be judged by the coordination environment and content of aluminum because of their amorphous and thick pore wall.

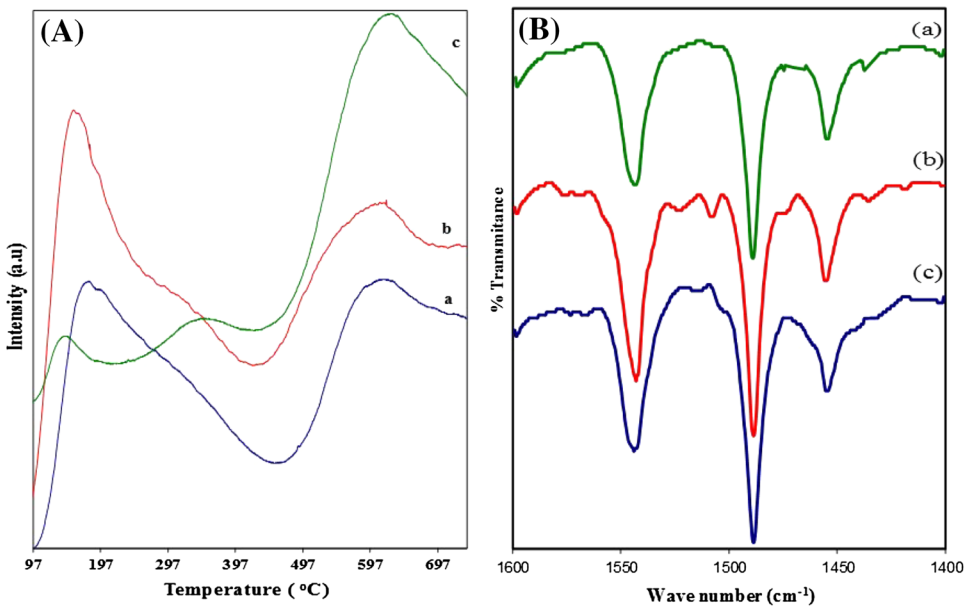

Fig. 7 **a** NH_3-TPD profiles, **b** Py-FTIR spectra of (*a*) AlSBA-15(3), (*b*) AlSBA-15(7) and (*c*) AlSBA-15(15) materials with different nSi/mAl ratios

Table 2 The total number of acid sites of AlSBA-15 materials synthesized at various *n*Si/*n*Al ratios

Sample	Total number of acid sites (mmol g^{-1})[a]	Number of acid sites (μmol g^{-1})[b]		B/L ratio[b]
		Brönsted (B)	Lewis (L)	
AlSBA-15(3)	0.956	13	9	1.4
AlSBA-15(7)	1.108	48	21	2.3
AlSBA-15(15)	1.057	31	17	1.8

[a]NH_3-TPD analysis

[b]FTIR spectra after pyridine adsorption

NH_3-TPD technique does not supply any information differentiate Lewis versus Brønsted acid sites. The acid site distribution on all AlSBA-15 samples containing adsorbed pyridine as a probe molecule was analyzed by FT-IR spectroscopy. The FT-IR spectra of the materials after pyridine adsorption are displayed in Fig. 7b. All the AlSBA-15 with various nSi/mAl ratios contain Lewis acid sites (LAS) and Brønsted acid sites (BAS), as confirmed by the characteristics bands at 1450 and 1545 cm^{-1}, respectively. In addition, the band at 1485 cm^{-1} indicates the formation of the adjacent Lewis and Brønsted acid sites [36]. The ratio of the concentrations of Brønsted and Lewis acid sites (B/L) for each catalyst was determined as shown in Table 2, by calculating the intensities of the FTIR bands corresponding to the respective acid sites [37]. It worth noting that AlSBA-15(7) show an increase of B/L ratio among the other materials with greater number of Bronsted acid sites, thus increasing the B/L ratio.

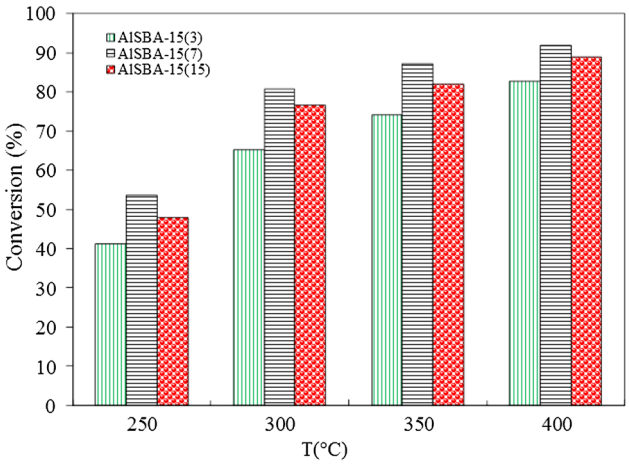

Fig. 8 Effect of Si/Al ratio on the cumene Cracking over AlSBA-15 at different reaction temperatures

3.2 Catalytic activity

The cumene cracking as a probe reaction was adopted to estimate the acidity of the materials, which has been cited in the literature to be a reaction for the simultaneous estimation of Brønsted (BAS) as well as Lewis acidity (LAS). The reactions that take place during the cumene cracking are categorized as dealkylation (cracking) which produces benzene and propene over BAS and dehydrogenation gives α-methyl styrene over LAS (Scheme 2) [38]. As shown in Fig. 8, all materials have considerable activity although their different textural characteristics and the catalytic performance based on robustly on the Si/Al ratio. AlSBA-15(3) shows low catalytic activity with 39% conversion in this reaction whereas; AlSBA-15(7) and AlSBA-15(15)

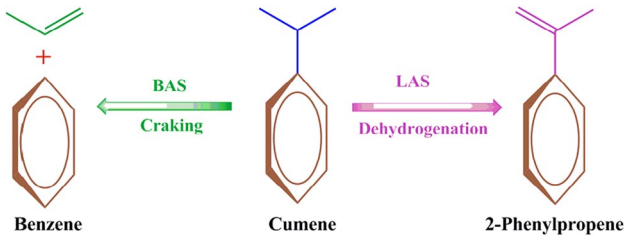

Scheme 2 Cumene cracking over Brønsted and Lewis acid sites

samples show high catalytic activities with a conversion of 55 and 47%, respectively, at 250 °C. The catalytic cumene cracking is increased with increasing temperature and reach 92% for AlSBA-15(7) at 400 °C. These results indicate that AlSBA-15(7) and AlSBA-15(15) have good catalytic activities than AlSBA-15(3) due to their high acidity. Furthermore, the analysis of the cracked cumene was found to be benzene and propene, confirming that the active sites of these kind materials are Bronsted type.

A brief comparison of the catalytic performance of various catalysts for Cumene cracking taking into consideration the reaction conditions is given in Table 3 (data collected from various published papers) [39–43]. Summing up, the reported results within the frame of present work do reflect that Al-Substituted SBA-15 mesoporous materials offers new, exciting opportunities for heterogeneous solid acid catalyst in comparison to the others.

The esterification of acetic acid with butyl alcohol is an electrophilic substitution reaction. The reaction is relatively slow and needs activation either by high temperature or by an acid catalyst in order to achieve the equilibrium conversion with a reasonable amount. The effect of various parameters such temperature and nSi/mAl ratios on the esterification reaction over AlSBA-15 were investigated. The reaction was examined over AlSBA-15(3), AlSBA-15(7) and AlSBA-15(15) catalysts at 80 and 100 °C. The reactants molar ratio (butyl alcohol/acetic acid) were maintained at 1:1. The main product was only butyl acetate with 100% selectivity. The results of catalytic performance are compared in Fig. 9. The results revealed that the percentage yield of butyl acetate increases with an increase in the reaction temperature from 80 to 100 °C. This suggests that the increase in reaction temperature favors the formation of electrophile for nucleophilic attack by butyl alcohol leading to the formation of ester (butyl acetate). The esterification over AlSBA-15(7) shows the highest catalytic activity and more pronounced with 30% conversion and 100% selectivity towards n-butyl acetate as compared to that of AlSBA-15(3), and AlSBA-15(15). The enhancement in the activity of AlSBA-15(7) is attributed to a large number of acid sites, high surface area and large pore diameter of the support, which helps the accessibility of the acidic protons for the reactant molecules. However, the observed decrease in the activity of AlSBA-15(3) could be tentatively attributed to both the decrease in the specific surface area and the surface acidity. These results suggested that Al acted as the significant catalytically active sites of AlSBA-15 samples. Although the mechanism of homogeneously catalyzed liquid phase esterification is long known there is still no clarity regarding the heterogeneously catalyzed gas phase reaction. Chu et al. [44] found that the esterification mechanism of n-butanol with acetic acid catalyzed by immobilized dodecatungstosilicic acid on activated carbon proceeds via a protonated alcohol intermediate. However, a protonated carboxylic acid as the reaction intermediate has been proposed by other authors [45, 46]. However, the formation of ester with 100% selectivity can be accounted by the protonation of the acid as the rate determining step of the reaction [45].

4 Conclusions

Al-Substituted SBA-15 mesoporous materials with high aluminum content and superior structural order have been successfully fabricated by direct approach using ionic liquid and have been characterized adopting different

Table 3 Comparison of catalytic performance of various catalysts in the cumene cracking reaction

Catalyst	Reaction conditions	Conversion %	References
HY-0.67-48	0.26 g crushed to a particle size of 60–80 meshes catalysts in a fixed-bed reactor. Nitrogen carrier gas at flow of 3.0 L h. liquid cumene flow rate of =6.0 mL/h at 300 °C	88.3	[37]
FS-ATY-1	The reaction was in fixed-bed reactor. The catalysts were crushed to a particle size of 0.2–0.3 mm. Nitrogen was used as carrier gas at flow of 4.5–12 L h^{-1} @ 220 °C	~55	[38]
30MPZ	0.2 g catalyst was used @ 500 °C. 3 µL cumene reactant was injected in N2 gas stream (30 mL/min), into a microreactor attached on-line with gas chromatography	50	[39]
Y-Zeolite	200 mg of catalyst 20 vol% cumene/Ar, feed residence time of about 0.3 s @ 500 °C	97.2	[40]
HAlMSN	0.2 g of catalyst was placed in a quartz glass reactor. 36 µmol of cumene was injected over the catalyst @ 300 °C in hydrogen gas	55	[41]
AlSBA-15(7)	N_2/cumene ratio = 20 mL/mL, atmospheric pressure @ 400 °C	92	Present work

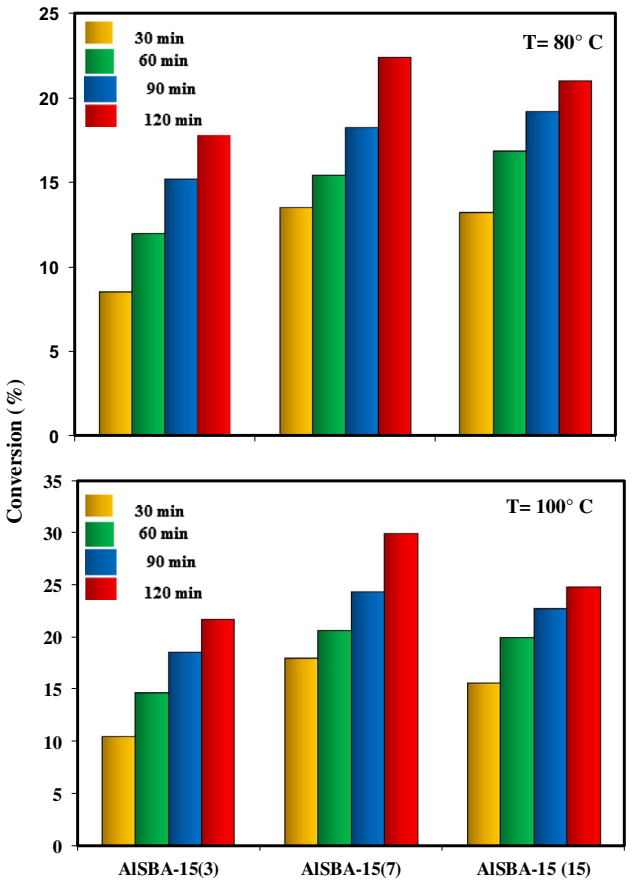

Fig. 9 Effect of nSi/mAl ratio over AlSBA-15 on the esterification reaction at 80 and 100 °C

techniques. XRD, N_2 sorption isotherms and ^{27}Al MAS NMR results confirm that AlSBA-15 can be synthesized under conditions of 3 < nSi/mAl > 15. All materials have considerable activity although their different textural characteristics towards esterification reaction and cumene cracking and the catalytic performance based on robustly on the nSi/mAl ratios.

References

1. M.R. Awual, Chem. Eng. J. **307**, 85–94 (2017)
2. M.R. Awual, Chem. Eng. J. **307**, 456–465 (2017)
3. M.R. Awual, Chem. Eng. J. **303**, 539–546 (2016)
4. M.R. Awual, Chem. Eng. J. **300**, 264–272 (2016)
5. M.R. Awual, M.M. Hasan, J. Ind. Eng. Chem. **21**, 507–515 (2015)
6. F. Marques Mota, P. Eliášová, J. Jung, R. Ryoo, Catal. Sci. Technol. **6**, 2735 (2016)
7. S.-W. Choi, W.-G. Kim, J.-S. So, J.S. Moore, Y. Liu, R.S. Dixit, J.G. Pendergast, C. Sievers, D.S. Sholl, S. Nair, C.W. Jones, J. Catal. **345**, 113 (2017)
8. C.F. Coriolano, G.F.S. Barbosa, C.K.D. Alberto, R.C.O.B. Delgado, K.K.V. Castro, A.S. Araujo, Petrol. Sci. Technol. **34**(7) 627 (2016)
9. R.D. Andrei, M. Mureseanu, M.I. Popa, C. Cammarano, F. Fajula, V. Hulea, Eur. Phys. J. Spec Top. **224**, 1831 (2015)
10. R. Chal, C. Gérardin, M. Bulut, S. van Donk, ChemCatChem **3**, 67–81 (2011)
11. R. Chal, C. Gerardin, M. Bulut, S. van Donk, ChemCatChem **3**, 67–81 (2010)
12. M.S. Abdel Salam, M.A. Betiha, S.A. Shaban, A.M. Elsabagh, R.M. Abd El-Aal, F.Y. El kady, Egypt J. Pet. **24**(1), 49–57 (2015)
13. A.E.R.S. Khder, H.M.A. Hassan, M.S. El-Shal, Appl. Catal. A **487**, 110–118 (2014)
14. H.M. Hassan, M.A. Betiha, S.K. Abd El Rahman, M. Mostafa, M. Gallab, J. Porous Mat. **23**, 133 (2016)
15. M. Guisnet, J.P. Gilson (eds.), *Zeolites for Cleaner Technologies, Catalytic Science Series*, vol 3. (Imperial College Press, London, 2002), p. 223
16. A. Corma, Curr. Opin. Solid State Mater. Sci. **2**, 63 (1997)
17. J.T. Pinnavaia, Z. Zhang, Stud. Surf. Sci. Catal. **117**, 23–36 (1998)
18. H. Wang, Y. Liu, T.J. Pinnavaia, J. Phys. Chem. B **110**, 4524–4526 (2006)
19. K.S. Triantafyllidis, A.A. Lappas, I.A. Vasalos, H. Wang, Y. Liu, T.J. Pinnavaia, Catal. Today **112**, 33–36 (2006)
20. S. Zeng, J. Blanchard, M. Breysse, Y. Shi, X. Shu, H. Nie, D. Li, Micropor. Mesopor. Mater. **85**, 297–304 (2005)
21. Y. Xia, R. Mokaya, J. Mater. Chem. **14**, 3427–3435 (2004)
22. J. Walker, J.K. Wood, J. Chem. Soc. Trans. **83**, 484 (1903)
23. A. Zecchina, S. Bordiga, G. Spoto, L. Marchese, G. Petrini, G. Leofanti, M. Padovan, J. Phys. Chem. **96**, 4985 (1992)
24. F. Kleitz, F. Bérubé, R.G. Nicolas, C.M. Yang, M. Thommes, J. Phys. Chem. C **114**, 9344 (2010)
25. A. Taguchi, F. Schüth, Micropor. Mesopor. Mater. **77**, 1 (2005)
26. D. Zhao, J. Feng, Q. Huo, N. Melosh, G.H. Frederickson, B.F. Chmelka, G.D. Stucky, Science **279**, 548 (1998)
27. D. Zhao, Q. Huo, J. Feng, B.F. Chmelka, G.D. Stucky, J. Am. Chem. Soc. **120**, 6024 (1998)
28. D. Zhao, Q. Huo, J. Feng, B.F. Chmelka, G.D. Stucky, J. Am. Chem. Soc. **120**, 6024.3 (1998)
29. A. Vinu, G. Satishkumar, K. Ariga, V. Murugesan, J. Mol. Catal. A **235**, 57 (2005)
30. K.S.W. Sing, D.H. Everett, R.A.W. Haul, L. Moscou, R.A. Pierotti, J. Ouquerol, T. Siemieniewska, Pure Appl. Chem. **57**, 603 (1985)
31. M. Imperor-Clerc, P. Davidson, A. Davidson, J. Am. Chem. Soc. **122**, 11925 (2000)
32. K.S.W. Sing, D.H. Everett, R.A.W. Haul, L. Moscou, R.A. Pierotti, J. Rouquerol, T. Siemieniewska, Pure Appl. Chem. **57**, 603 (1985)
33. A. Vinu, V. murugesan, W. Bohlmann, M. Hartmann, J. Phys. Chem. B **108**, 11496–11505 (2004)
34. N.Y. Topsoe, K. Pedersen, E.G. Derouane, J. Catal. **70**, 41 (1981)
35. L.J. Lobree, I.C. Hwang, J.A. Reimer, A.T. Bell, J. Catal. **186**, 242 (1999)
36. M.A. Betiha, H.M.A. Hassan, A.M. Al-Sabagh, A.S. Khder, E.A. Ahmed, J. Mater. Chem. **22**, 17551–17559 (2012)
37. R. Purova, K. Narasimharao, N.S.I. Ahmed, S. Al-Thabaiti, A. Al-Shehri, M. Mokhtar, W.J. Schwieger, J. Mol. Catal. A **406**, 159–167 (2015)
38. T. Chiranjeevi, G. Muthu Kumaran, J.K. Gupta, G. Murali Dhar, Thermochim. Acta **443**, 87 (2006)
39. Z. Liu, C. Shi, D. Wu, S. He, B. Ren, J. Nanotechnol. **148**, 6107 (2016)

40. Z. Qin, B. Shen, X. Gao, F. Lin, B. Wang, C. Xu, J. Catal. **278**, 266 (2011)
41. E.A. El-Sharkawy, A.S. Khder, A.I. Ahmed, Micropor. Mesopor. Mater. **102**,128 (2007)
42. N. Hosseinpour, Y. Mortazavi, A.A. Khodadadi, Appl. Catal. A **487**, 26 (2014)
43. M.R. Sazegar, A.A. Jalil, S. Triwahyono, R.R. Mukti, M. Aziz, M.A.A. Aziz, H.D. Setiabudi, N.H.N. Kamarudin, Chem. Eng. J. **240**, 352, (2014)
44. W. Chu, X. Yang, X. Ye, Y. Wu, J. Appl. Catal. A Gen. **145**, 125 (1996)
45. A.S. Khder, E.A. El-Sharkawy, S.A. El-Hakam, A.I. Ahmed, Catal. Commun. **9**, 769 (2008)
46. H.T.R. Teo, B. Saha, J. Catal. **228**, 174 (2004)